On the Radiation Chart.

On a Radiation Chart

By Giichi YAMAMOTO

Geophysical Institute, Faculty of Science, Tôhoku University

(Received April 25, 1952)

Abstract

Using reasonable values of absorption coefficient of water vapour and transmission function, a radiation chart which is similar in shape but different in principle to Kew chart was constructed. One of the charcteristics of the chart will be found in its improved treatment of CO_2 absorption, the correction of which being carried out using an auxiliary diagram. Examples of the computation of radiative flux using the chart are shown and discussed.

1. Introduction

Graphical methed of the computation of radiative flux in the atmosphere was originally investigated by MÜGGE and MÖLLER [1], and a radiation chart was constructed by MÖLLER basing on the investigation. ELSASSER [2] designed another chart which is now widely used in the United States. Recently ROBINSON [3] has constructed a new type of chart which he called Kew chart, and a similar chart with somewhat reasonable treatment of CO_2 absorption was presented by DEACON [4]. Among these, Kew chart and DEACON's will be most convenient in construction. However, they seem to be unsatisfactory in principle, as will be shown later. In this paper, new radiation chart which is theoretically reasonable and has similar construction to Kew chart will be described.

2. Transmission Function

By solving the equation of radiative transfer with boundary conditions that downward radiation is zero at the top of the atmosphere and upward radiation at the surface is equal to the black body radiation of the surface temperature, we have

$$U_\nu(z) = B_\nu(T_z) + \int_{T_z}^{T_0} \frac{dB_\nu(T)}{dT}\,\tau_f(l_\nu u)\,dT \quad (1),$$

$$D_\nu(z) = B_\nu(T_z) - B_\nu(T_\infty)\tau_f(l_\nu u_\infty) + \int_{T_z}^{T_\infty} \frac{dB_\nu(T)}{dT}\,\tau_f(l_\nu u)\,dT \quad (2),$$

where $U_\nu(z)$, $D_\nu(z)$ respectively are upward and downward fluxes of frequency ν (cm^{-1}) at height z, T_0, T_z, T_∞ respectively temperatures at the surface, the level z and the top of the atmosphere, $B_\nu(T)$ the black body flux of frequency ν at temperature T, u the precipitable water in the air column which is measured from the level z downward in equation (1) and upward in equation (2), u_∞ that from the level z to the top of the atmosphere, l_ν the generalized absorption coefficient of ELSASSER, $\tau_f(l_\nu u)$ the transmission function of a slab given by

$$\tau_f(l_\nu u) = 2\,[Ei_3(k_\nu u)]_{\text{average}} \quad (3),$$

where k_ν is the usual absorption coefficient and $Ei_3(x)$ is the third exponential integral, *i. e.*,

$$Ei_3(x) = \int_1^\infty e^{-xt}\,\frac{dt}{t^3} \quad (4).$$

ELSASSER [2] has obtained the transmission function for an idealized band of equal and equidistant lines, where k_ν is given by

$$k(\nu) = \frac{S}{d}\,\frac{\sinh\beta}{\cosh\beta - \cos s} \quad (5),$$

$$s = \frac{2\pi\nu}{d}, \qquad \beta = \frac{2\pi a}{d} \quad (6),$$

and S is the total intensity of a line, d the distance of neighbouring lines, a the half-

width. According to ELSASSER the transmission function τ_I of a column is given by

$$\tau_I = [e^{-k_\nu u}]_{\text{average}} = \frac{1}{2\pi}\int_{-\pi}^{+\pi} e^{-k(s)u}\,ds$$

$$= 1 - \sinh\beta \int_0^{\frac{Su}{d\sinh\beta}} e^{-y\cosh\beta}\, J_0(iy)dy \quad (7),$$

where $J_0(iy)$ is BESSEL function of zeroth order with an imaginary argument. For large value of u, equation (7) takes following approximate form, *i. e.*,

$$\tau_I = 1 - \phi\left(\sqrt{\frac{l_\nu u}{2}}\right) \quad (8),$$

where $\phi(x) = \frac{2}{\sqrt{\pi}}\int_0^x e^{-x^2}\,dx$ and $l_\nu = \frac{S\beta}{d}$ = generalized absorption coefficient of ELSASSER. Introducing (7) in (3), we have

$$\tau_I = 1 - 2\sinh\beta \int_1^\infty \frac{dt}{t^3}\int_0^{\frac{Sut}{d\sinh\beta}} e^{-y\cosh\beta}\, J_0(iy)dy \quad (9).$$

Integrating by parts, we have

$$\tau_I = 1 - \sinh\beta \int_0^{\frac{Su}{d\sinh\beta}} e^{-y\cosh\beta}\, J_0(iy)dy$$

$$-\sin\beta\left(\frac{Su}{d\sinh\beta}\right)^2$$

$$\times \int_{\frac{Su}{d\sinh\beta}}^\infty \frac{1}{y^2}\, e^{-y\cosh\beta}\, J_0(iy)dy \quad (10).$$

Equation (10) is the general formula of τ_I for ELSASSER's idealized band. If β is small we can put $\sinh\beta = \beta$, $\cosh\beta = 1 + \frac{\beta^2}{2}$, and we have

$$\tau_I = 1 - \beta\int_0^{\frac{l_\nu u}{\beta^2}} e^{-y(1+\frac{\beta^2}{2})}\, J_0(iy)dy$$

$$-\frac{(l_\nu u)^2}{\beta^3}\int_{\frac{l_\nu u}{\beta^2}}^\infty \frac{1}{y^2}\, e^{-y(1+\frac{\beta^2}{2})}\, J_0(iy)dy \quad (11).$$

For large value of u equation (11) is transformed to

$$\tau_I = \frac{2}{3} - \frac{1}{\sqrt{\pi}}\sqrt{\frac{l_\nu u}{2}}\left(2\,\frac{l_\nu u}{2} - 1\right)e^{-\frac{l_\nu u}{2}}$$

$$-\left\{\frac{4}{3}\left(\frac{l_\nu u}{2}\right)^2 - 1\right\}\left\{1 - \phi\left(\sqrt{\frac{l_\nu u}{2}}\right)\right\} \quad (12).$$

Equation (12) was originally derived by ELSASSER.

Recently COWLING [5] has calculated numerically the mean transmission for several regions in the rotation band of water vapour. He has shown that ELSASSER's transmission function expressed by equation (8) disagrees with transmission curves, obtained from FOWIE's [6] and ADEL's [7] measurements and also from his calculation, for both small and large values of u. The reason for this discrepancy is to be attributed to the irregularity in strength and spacing of the absorption lines in the water vapour band. For large values of u this discrepancy is fatal to ELSASSER's transmission function. However, for small values of u, it is well known that equation (8) is only a bad approximation to ELSASSER's transmission function which is rightly expressed by equation (7), so that COWLING's comparison does not necessarily mean true criticism on ELSASSER's formula for small values of u. For extremely small values of u, equation (7) becomes as follows:

$$\tau_I = 1 - Su/d \quad (13),$$

which means that the absorption is proportional to the product of water path u and the mean absorption coefficient, S/d. This circumstance will probably be true in the actual band too. Therefore, we may say that ELSASSER's trasmission function expressed by equation (7) will approximately agree with the true transmission function for small values of u. On this consideration I have calculated the values of τ_I of equation (7) by graphical integration assuming that $\beta = 0.2$(*i. e.*, $a = 0.1$ and $d = 3$), which I think to be appropriate values for the rotation band of water vapour at normal conditions. The values of τ_I shown in table 1 which correspond to the values of $l_\nu u/2$ smaller than 0.1 are the result of the computation.

Now COWLING has also shown that transmission curves take somewhat different forms for different regions of the band. However,

Table 1. Values of τ_I and τ_f of water vapour used in this paper

$l_\nu u/2$	τ_I	τ_f	$l_\nu u/2$	τ_I	τ_f
0.0001	0.999	0.998	0.06	0.738	0.648
0.0003	0.997	0.994	0.1	0.658	0.560
0.0006	0.994	0.988	0.3	0.457	0.372
0.001	0.990	0.982	0.6	0.330	0.255
0.003	0.972	0.952	1	0.242	0.180
0.006	0.948	0.914	3	0.083	0.060
0.01	0.918	0.876	6	0.032	0.022
0.03	0.824	0.752	10	0.010	0

he also considered that it is convenient to use a single transmission curve in atmospheric work to avoid complication. and for the purpose he has chosen the curve XII of fig. 3 of his paper to be the mean transmission curve. His curve XII is now drawn in fig. 1, at the place

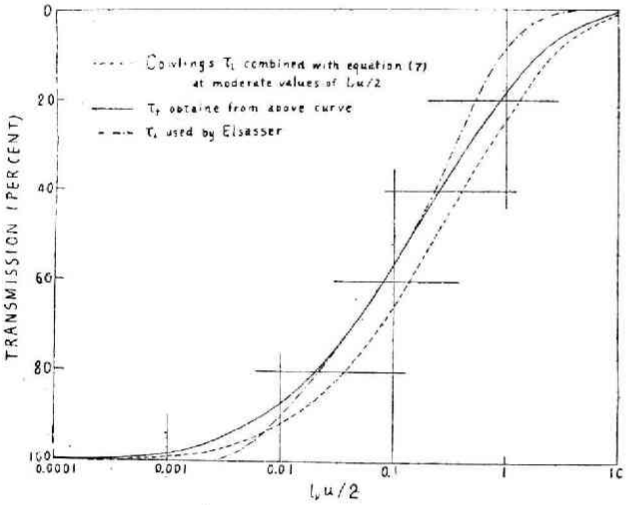

Fig. 1 Transmission curves

where it coincides with ELSASSER's transmission values shown in table 1 at moderate values of $l_\nu u/2$. The curve thus obtained gives COWLING's transmission curve of a column as function of $l_\nu u/2$. The values of τ_I in table 1 which correspond to the values of $l_\nu u/2$ larger than 0.1 are obtained from the curve.

Next, it is necessary to obtain the transmission curve of a slab, τ_f. It was shown by ELSASSER that $\tau_f(u)$ is nearly equal to $\tau_I(1.66\,u)$. Recently, however, more plausible relation between τ_I and τ_f was obtained by YAMAMOTO [8] for the water vapour band. So the values of τ_f were calculated from those of τ_I (in table 1) using the relation derived by YAMAMOTO. The obtained values of τ_f for the water vapour band are also shown in table 1 and fig. 1. For the sake of comparison ELSASSER's curve of τ_f which he actually used in constructing his radiation chart is also shown in fig. 1. Apart from the incorrectness of his curve for large values of $l_\nu u/2$, it also depart from our curve for small values of $l_\nu u/2$. His curve was derived from his equation (12) with some correction for small thickness. However, as our τ_f-curve is a reasonable consequeuce of COWLING's τ_I-curve or of general equation (10), it seems that his correction to equation (12) for small thickness is inadequate.

3. Absorption Coefficient of Water Vapour

The next step to do is to know the values of l_ν for water vapour bands. As the transmission function τ_I $(l_\nu u/2)$ is already known, the value of l_ν at frequency ν can easily be determined if the value of τ_I is measured for known values of u and ν. In this context difficulty rather lies in the selection of appropriate experimental results, because considerable numbers of experiments were hitherto carried out at different conditions and subsequently with discrepancies in results. For the vibration band around 6.3 μ we availed FOWLE's [9] measurements to determine l_ν. For the intermediate region 8-13 μ ADEL and LAMPLAND's [10] measurments were taken as standard. For the part of rotation band between 17 and 24 μ RANDALL and WEBER's [11] measurements at room temperature (26.3°C) were taken as standard. Their mesurments on steam were not taken into account, because the value of halfwidth on steam will be different from that at ordinary conditions. WEXLER [12] had already calculated the values of k_ν from RANDALL and WEBER's

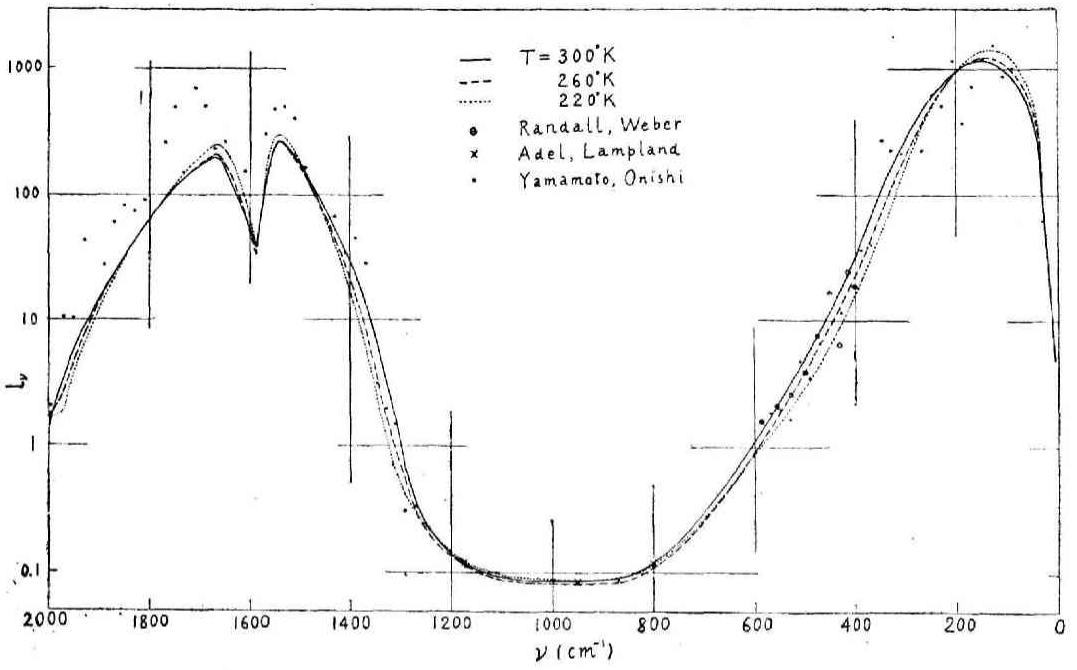

Fig. 2 Generalized absorption coefficient of water vapour

measurements. However, here, we have calculated the average values of l_ν from mean absorption of each 25 cm^{-1} interval of their original data.

In the far infra-red region of the rotation band, as yet no reliable experimental data are known, so that the values of l_ν calculated by YAMAMOTO and ONISHI [13] for $T = 300°$ K were taken into account. As will be seen in fig. 2, in the range between 17-24 μ the theoretical values of YAMAMOTO and ONISHI agree fairly well with the values obtained from RANDALL and WEBER's measurements, which will to some extent warrant for the utilization of the theoretical values in the far infra-red region until reliable experimental data will be available. The smoothed curve of generalized absorption coefficient at $T = 300°$ K which covers entire regions from the 6.3 μ band to the rotation band are thus obtained as shown in fig. 2. It will be noticed that in the vibration band the agreement between computed and observed values are not so good, as was pointed out by GOODY and ROBINSON [14]; computed values being generally larger than observed values.

Now absorption coefficient is known to depend upon pressure. It was recently shown by COWLING [5] that ELSASSER's pressure correction which replaces a quantity u of water vapour at pressure p by a quantity $u\sqrt{p/p_0}$ at standard pressure p_0 is in most cases an under-correction and that true correction is often nearer to replacing u by up/p_0. So the latter alternative was assumed in the present paper.

The temperature effects on absorption coefficient are scarcely known experimentally and we are only able to infer them theoretically. First, according to LORENTZ's theory the line-width varies with temperature as proportional to $T^{-1/2}$. Second, temperature changes affect the populations of the different energy-levels : the high energy-levels, which contribute most to band wing absorption, are but scanty occupied at low temperatures. A decrease in temperature therefore leads to an increase in absorption near a band centre but makes the absorption cut-off at the wings of

the band sharper. ELSASSER [2] and COWLING [5] have discussed the temperature effects on absorption. YAMAMOTO and ONISHI [13] have also calculated the values of l_ν at following three conditions, *i.e.*, at $T=300°$K and relative humiaity of 60%, $T = 260°$K and infinitesimal vapour pressure and $T=220°$K and infinitesimal vapour pressure. In this calculation the strengths of absorption lines have been calculated by the method of KING, HAINER and CROSS [15], and the absorption line was assumed to take the shape proposed by VAN VLECK and WEISSKOPF [16], and the half-width was assumed to depend on air pressure according to LORENTZ theory and to depend on water vapour pressure according to BECKER and AUTLER's theory [17]. Smoothed curves of l_ν at $T = 260°$ and $220°$ K shown in fig. 2 were obtained from the curve at $T = 300°$ K by supplementing corrections based on YAMAMOTO and ONISHI's computed values.

4. Construction of New Radiation Chart

New chart is in principle a transformation of ELASSER's chart taking different quantities as abscissa and ordinate. However it treats water vapour absorption and CO_2 absorption separately. At first water vapour absorption alone is considered and the treatment of CO_2 absorption will be shown in the next section.

From equations (1) and (2) total upward and downward fluxes U and D are given by

$$U = \int_0^\infty U_\nu d\nu = \int_0^\infty B_\nu(T_z)d\nu + \int_0^\infty \int_{T_z}^{T_0} \frac{dB_\nu(T)}{dT} \tau_f(l_\nu u)dTd\nu \quad (14),$$

$$D = \int_0^\infty D_\nu d\nu = \int_0^\infty B_\nu(T_z)d\nu - \int_0^\infty B_\nu(T_s)\tau_f(l_\nu u_s)d\nu - \int_0^\infty \int_{T_\infty}^{T_z} \frac{dB_\nu(T)}{dT} \tau_f(l_\nu u)dTd\nu \quad (15),$$

where

$$\int_0^\infty B_\nu(T)d\nu = B(T) = \sigma T^4 \quad (16),$$

σ being STEFAN's constant.

Now we put

$$\int_0^\infty \frac{dB_\nu(T)}{dT} \tau_f(l_\nu u)d\nu = \frac{dB(T)}{dT} \overline{\tau_f\{u(T)\}} \quad (17),$$

where

$$\frac{dB}{dT} = \int_0^\infty \frac{dB_\nu(T)}{dT} d\nu = 4\sigma T^3 \quad (18),$$

$\overline{\tau_f\{u(T)\}}$ is the weighted mean of $\tau_f(l_\nu u)$, so that it is a known function of u(or T) and free from l_ν. Introducing (17) into (14) and (15), we have

$$U = B(T_z) + \int_{T_z}^{T_0} \frac{dB(T)}{dT} \overline{\tau_f\{u(T)\}}\, dT = B(T_z) + \int_{B(T_z)}^{B(T_0)} \overline{\tau_f\{u(T)\}}\, dB \quad (19),$$

$$D = B(T_z) - \int_0^\infty \int_0^{T_\infty} \frac{dB_\nu(T)}{dT} \tau_f(l_\nu u_\infty)dTd\nu - \int_{T_\infty}^{T_z} \frac{dB(T)}{dT} \overline{\tau_f\{u(T)\}}\, dT = B(T_z) - \int_0^{B(T_\infty)} \overline{\tau_f\{u_\infty(T_\infty)\}}\, dB - \int_{B(T_\infty)}^{B(T_z)} \overline{\tau_f\{u(T)\}}\, dB \quad (20).$$

Equations (19) and (20) give idea on our radiation chart, that is, $B(T)$ is taken as abscissa and $\overline{\tau_f\{u(T)\}}$ as ordinate in the chart. The values of $\overline{\tau_f\{u(T)\}}$ were computed from equation (17) for $T = 300°$, $260°$, $220°$ and $100°$ K using respective values of l_ν in fig. 2,

Table 2 Values of $\overline{\tau_f\{u(T)\}}$

Water path u (cm)	300° K	260° K	220° K	100° K
0.0001	0.972	0.972	0.968	0.848
0.0003	0.946	0.949	0.943	0.749
0.0006	0.924	0.928	0.921	0.675
0.001	0.904	0.910	0.902	0.615
0.003	0.848	0.858	0.851	0.482
0.006	0.808	0.821	0.812	0.403
0.01	0.777	0.790	0.781	0.350
0.03	0.698	0.713	0.702	0.260
0.06	0.643	0.657	0.643	0.198
0.1	0.599	0.612	0.597	0.165
0.3	0.500	0.510	0.488	0.103
0.6	0.432	0.439	0.413	0.074
1	0.379	0.384	0.356	0.056
3	0.258	0.259	0.234	0.027
6	0.187	0.188	0.168	0.015
10	0.140	0.140	0.121	0.010
30	0.059	0.059	0.049	0.003

for the case of 100° K the values of l_ν at T = 220° K being used. The results of the computation are listed in table 2 and the radiation chart is constructed from these data as shown in fig. 3, in which isotherms, T = const. and curvs of constant water path, u = const. are drawn as auxiliary lines.

Upward flux U of equation (19) is then given by areas (1) + (2) + (3) + (4) as shown schematically in fig. 4, and downward flux D of equation (20) is given by area (1) and net flux $U-D$ is given by area (2)+(3)+(4).

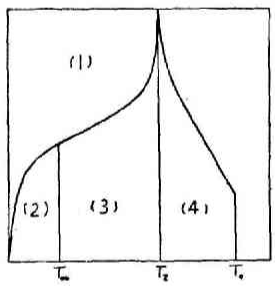

Fig. 4
Graphical computation of the radiative flux of water vapouralone

We shall now give a remark on Kew and DEACON's chart. They are similar to our chart, but essential difference is that they use emissivity ε_f or $1-\varepsilon_f$ as ordinate instead $\bar{\tau}_f$ in our chart. From the definition of emissivity of a slab which is given by

$$\varepsilon_f\{u(T)\} = 1 - \int_0^\infty B_\nu(T)\tau_f(l_\nu u)\, d\nu / B(T) \quad (21),$$

we see that $1-\varepsilon_f\{u(T)\}$ is the weighted mean value of τ_f with $B_\nu(T)$ as the weight function, while in the case of $\overline{\tau_f\{u(T)\}}$ the weight function is $dB_\nu(T)/dT$. So that the values of $1-\varepsilon_f$ and $\bar{\tau}_f$ have some difference. ROBINSON and DEACON further assumed that ε_f is independent of temperature. Even with this assumption $1-\varepsilon_f$ can not be considered to be equal to $\bar{\tau}_f$.

Differetiating equation (21) with T we have

$$\int_0^\infty \frac{dB_\nu(T)}{dT}\tau_f(l_\nu u)d\nu + \int_0^\infty B_\nu(T)\frac{d\tau_f(l_\nu u)}{dT}\, d\nu$$

$$= \frac{dB}{dT}\left\{1-\varepsilon_f\{u(T)\}\right\} - B(T)\frac{d\varepsilon_f\{u(T)\}}{dT} \quad (22).$$

If we assume as ROBINSON and DEACON did that ε_f is independent of temperature, then the last term of (22) vanishes. But evidently $\int_0^\infty d_\nu(T)\frac{d\tau_f\{l_\nu u(T)\}}{dT}\, d\nu$ does not vanish. So that upward flux of equation (14), for instance, will be given by

$$U = B(T_z) + \int_{B(T_z)}^{B(T_0)}\{1-\varepsilon_f\{u(T)\}\}\, dB - \int_0^\infty\int_{T_z}^{T_0} B_\nu(T)\frac{d\tau_f\{l_\nu u(T)\}}{dT}\, dT d\nu \quad (23).$$

The last term of equation (23) is neglected by ROBINSON and DEACON. But there is no reason to neglect this term. Transforming variable from T to u, we have

$$\frac{d\tau_f\{l_\nu u(T)\}}{dT}\, dT = \frac{d\tau_f\{l_\nu u(T)\}}{du}\, du < 0 \quad (24),$$

because τ_f is a decreasing function of u. Thus it will be said that their charts are at least principally in error, and that from equations (23) and (24), as far as they used correct value of emissivity, the values of U calculated by their charts are somewhat underestimated, and those of D overestimated. In order to illustrate the difference between $1-\varepsilon_f$ and $\bar{\tau}_f$, we computed the values of $1-\varepsilon_f$ which correspond to T = 293° K and they were compared with the values of $\bar{\tau}_f$ at 300° K as shown in fig. 5.

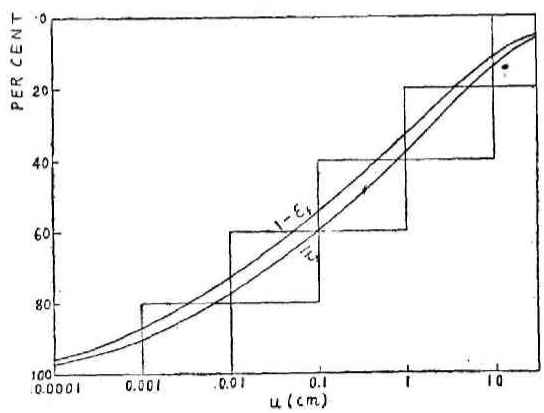

Fig. 5 $\bar{\tau}_f$ at 300° K and $(1-\varepsilon_f)$ at 293° K

Although minor difference will be caused due to the differently assumed temperatures on each computation, the difference of the values shown in fig. 5 will mainly be essential one

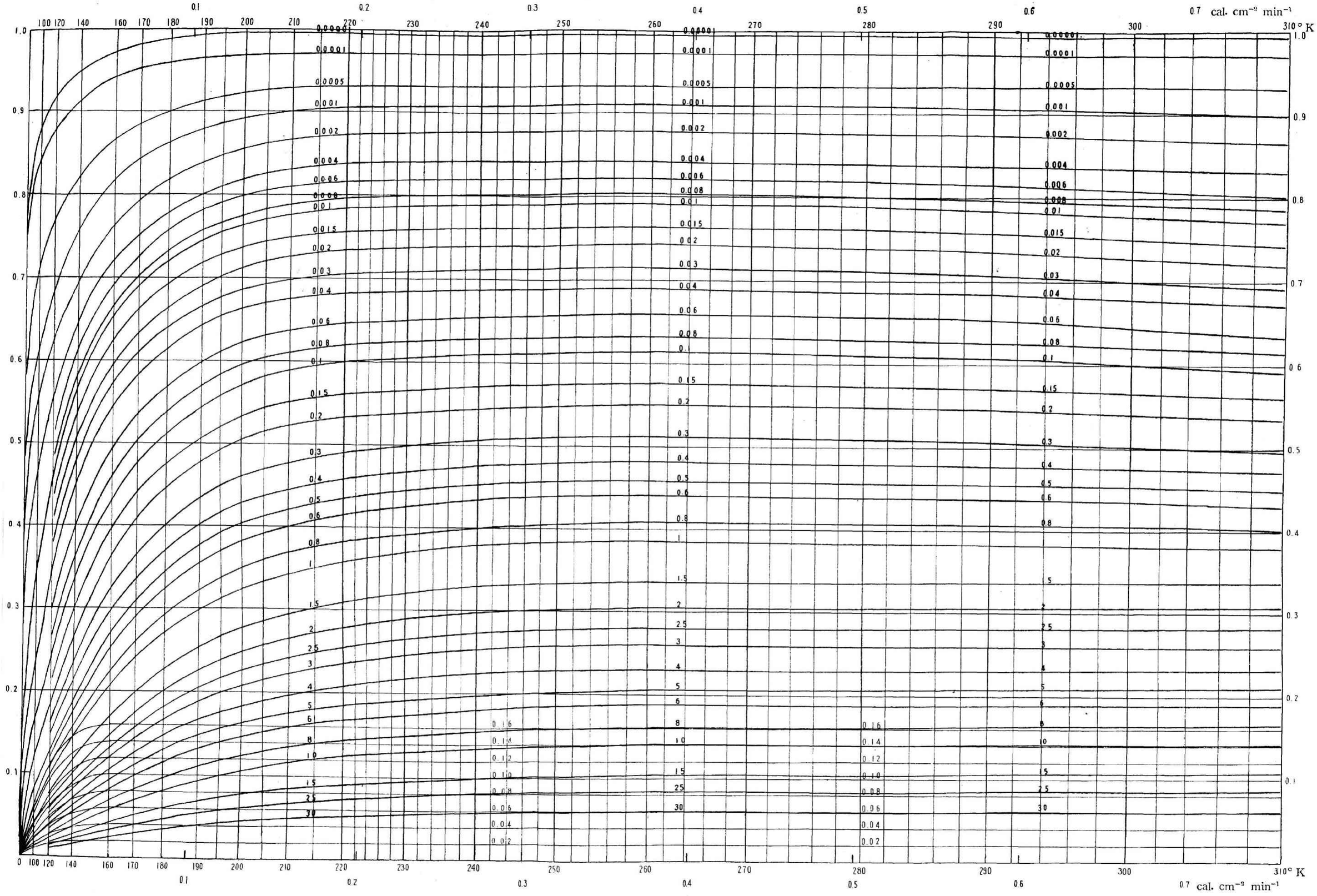

Figure 3. Radiation chart. Ordinate is $\overline{\tau_f\{u(T)\}}$ and abscissa $B(T)$. Isotherms and constant u curves are drawn as auxiliary curves.

Nearly horizontal curves in the lower part of the chart are constant $\Delta\tau_f\{u, u_{CO_2}\}$ curves for CO_2 correction.

due to the difference of the weight functions on both cases. The order of error which will enter into the computation of U or D by using $1-\varepsilon_f$ instead of $\bar{\tau}_f$ as ordinate of the chart, will be presumed from fig. 5 to be about $4 \sim 5$ per cent of the black body flux of the level. Actually, however, according to ROBINSON, the values of the downward flux at the surface computed from Kew chart agree very well with his obserations. The reason is not evident, but at least it will be said that the values of ε_f used by ROBINSON are different from ours and CO_2 corrections of him also differ from ours.

5. Correction of CO_2 Absorption

ELSASSER and ROBINSON assumed in their charts that CO_2 absorption is complete for the range from 584 to 725 cm^{-1} (17.1 - 13.3 μ) regardless of the quantities of water vapour and carbon dioxide. DEACON made some improvement in this context but his treatment is not satisfactory. Essentially the absorption of mixed gases will not be expressed reasonably in a single chart. So I have tried to make CO_2 correction using another diagram.

Empirical formula for the transmission function of far infra-red CO_2 band was proposed by CALLENDAR [18]. Recently KAPLAN [19] has shown that for 14 - 16 μ the theoretical calculation of absorption agrees with observed results of MARTIN and BARKER [20] and of RUBENS and LADENBURG [21]. It is regretted that his calculation covers only the range 14 - 16 μ. In his paper KAPLAN points out that RUBENS and LADENBURG's experiment was carried out with apparatus of poor resolution which would result apparently too much high values of absorption at the extremities of the band and correspondingly small absorption of 14 - 16 μ for large path lengths. However, at present, we can obtain no more experimental or theoretical absorption curves which will cover entire CO_2 bands in the far infra-red than those compiled by CALLENDAR. So in this paper, transmission values which are listed in table 1 of CALLENDAR's paper are used. These are reproduced in fig. 6.

Next, in the computation of atmospheric absorption, the transmission of a slab is necessary. In this context, to avoid laborous treatment, we assumed that the transimission of a slab of thickness u is equivalent to that of a column of length 1.5 u. The transmission curves of a slab thus obtained are also shown in fig. 6. The unit of CO_2 thickness has been taken as one cm of CO_2 column at normal pressure and temperature.

It is further assumed that the resultant transmissoin of a slab containing both water vapour and carbon dioxide is given by the product of individual transmissions. Then the correction due to carbon dioxide on $\overline{\tau_f(u)}$ of water vapour alone will be given by

$$\int_0^\infty \frac{dB_\nu(T)}{dT}\left\{\tau_f(l_\nu u)-\tau_f(l_\nu u)\cdot\tau_f(u_{CO_2})\right\}d\nu = \frac{dB(T)}{dT}\overline{\Delta\tau_f(u,u_{CO_2})} \qquad (25),$$

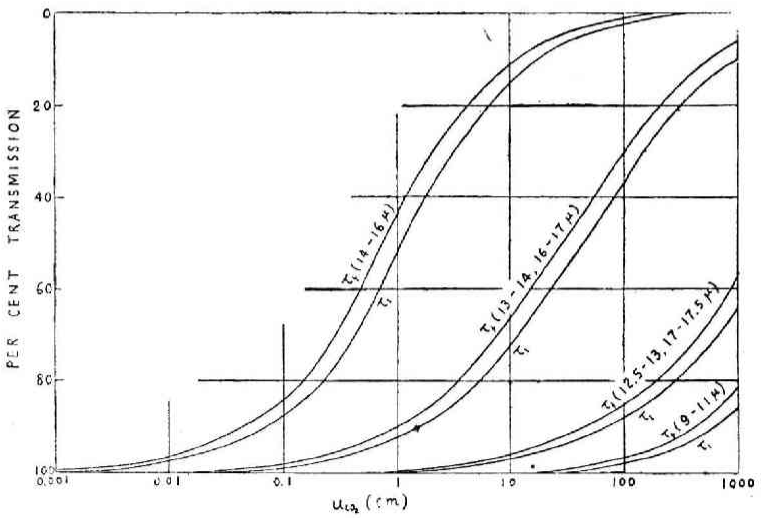

Fig. 6 Transmission curves of carbon dioxide

where $\tau_f(u_{CO_2})$ is the transmission of CO_2, u_{CO_2} is the thickness of CO_2 and $\overline{\Delta\tau_f(u, u_{CO_2})}$ is the amount of CO_2 correction which must be subtracted from $\overline{\tau_f(u)}$ in the radiation chart. The values of $\overline{\Delta\tau_f(u, u_{CO_2})}$ (fig. 7) are computed using PLANCK's energy curve and absorption coefficient of water vapour at 300°K and CALLENDAR's absorption curves which correspond to room temperatures. The temperature dependence of $\overline{\Delta\tau_f(u, u_{CO_2})}$ was neglected. However, at extremely low temperatures PLANCK's energy curve shifts to far infra-red, which will cause decrease of CO_2 absorption. To compensate this effect constant-$\overline{\Delta\tau_f(u, u_{CO_2})}$ curves, which coincide with constant-$\bar{\tau}_f$ lines in the radiation chart of fig. 3 at moderate temperatures, are curved down below $T = 160°$ K as shown in fig. 3. CO_2 correction is, thus, to be plotted on the lower part of the radiation chart. Fig. 8 shows the schematic view of the radiation chart in which both $u - T$ relation and CO_2 correction are drawn. Upward radiation at the level z is then given by areas (1)+(2)+(3)+(4)+(5)+(6), downward radiation by areas (1)+(5)+(6) and net flux by areas (2)+(3)+(4).

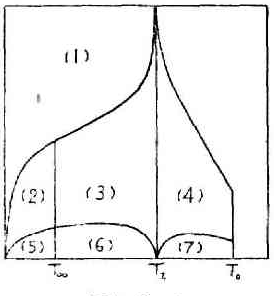

Fig. 8
Graphical computation of the radiative flux with CO_2 correction

In the atmosphere the variations of CO_2 content with place and season are rather small. So it will not be superflous to show the mean vertical distribution of CO_2 in the atmosphere. The volume per cent of CO_2 in the atmosphere is assumed to be constant throughout the air column, and its surface value to be 0.00032 or the partial pressure of CO_2 at the surface to be 0.32 mb. Then the reduced path of CO_2 from the surface to any height is approximately given by

$$u_{CO_2} = \frac{\rho_0}{\rho_{N.P.T}} \int_0^z e^{-0.276\times10^{-5}z}\, dz = \frac{32}{0.276}\left(1 - e^{-0.276\times10^{-5}z}\right) \quad (26),$$

where ρ_0 is the density of CO_2 at the surface, $\rho_{N.P.T}$ is that at normal pressure and temperature, z is the height in cm, the variation of pressure with height being assumed to be : $p = p_0\, e^{-0.138\times10^{-5}z}$. Values of u_{CO_2} for several heights are shown in table 3.

Table 3
The reduced path of CO_2 in the air column

Height (km)	u_{CO_2} (cm)	Height (km)	u_{CO_2} (cm)
0	0	6.0	93.8
0.1	3.2	7.0	99.2
0.2	6.2	8.0	103.3
0.5	15.0	9.0	106.4
1.0	28.0	10.0	108.7
1.5	39.3	11.0	110.5
2.0	49.2	12.0	111.7
2.5	57.8	13.0	112.8
3.0	65.3	14.0	113.5
3.5	71.8	15.0	114.2
4.0	77.5	16.0	114.6
4.5	82.5	20.0	115.5
5.0	86.8	∞	116.0

6. Emissivity of Water Vapour

So far we have described on the construction of our chart. Now we must check the validity of the chart. Using the values of l_ν and τ_f already described we can compute the emissivity of a column of water vapour, ε_f, which is defined by

$$\varepsilon_f(u, T) = 1 - \frac{\int_0^\infty B_\nu(T)\tau_f(l_\nu u)d\nu}{\sigma T^4} \quad (27).$$

This computation will be useful as an indirect check on the validities of the values of τ_f and l_ν, because the emissivity of water vapour was measured by FALKENBERG [22], ELSASSER [23]. Therefore the compution of the emissivity at 20° C was carried out using the values of l_ν at 300° K and the result was drawn in fig. 9, which was originally compiled by ELSASSER except our curve. It will be seen that our computed curve is in good agreement

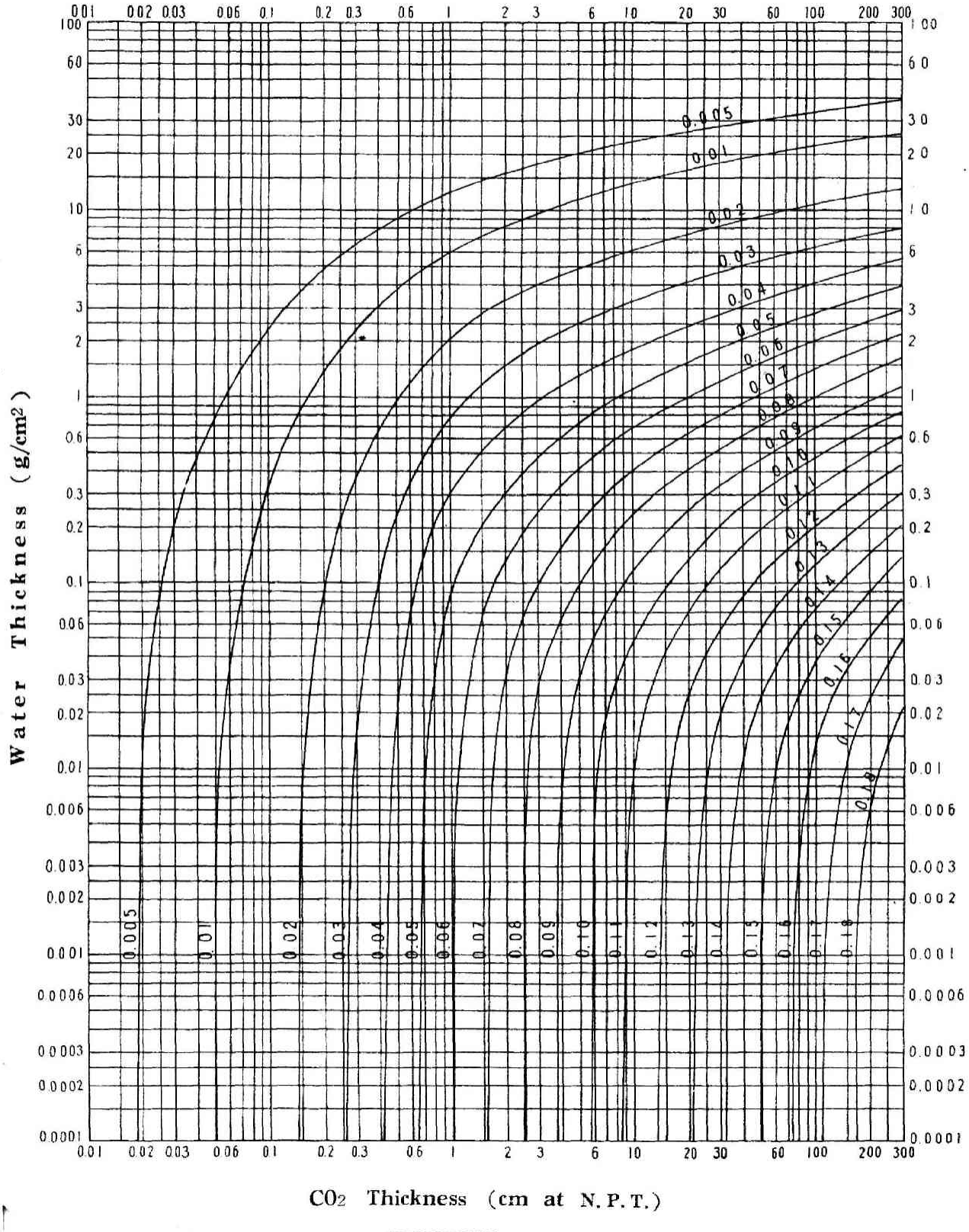

Figure 7. Diagram of $\overline{\Delta\tau_f(u, u_{CO_2})}$ as functions of u and u_{CO_2}

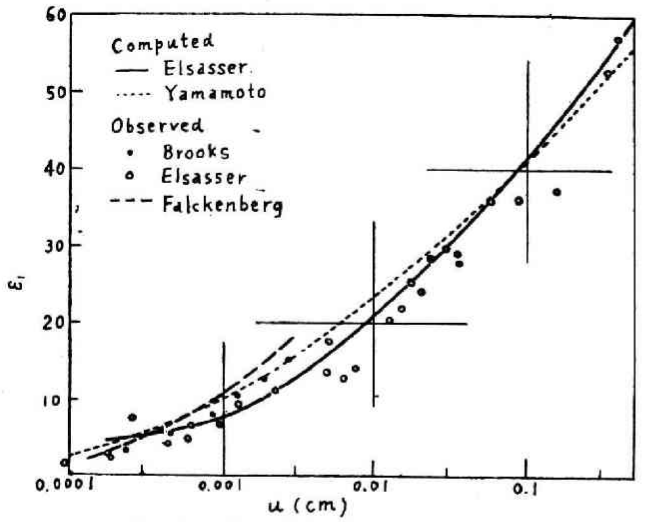

Fig. 9 Emissivity of column of water vapour without CO_2

with observed values for small and moderat values of u.

For large values of u there are no direct measurements of emissivity in the laboratory. However, F. A. BROOKS [24] and ROBINSON [3] have obtained the emissivity curves from observations of downward radiation in the atmosphere, which necessarily correspond to a mixture of water vapour and carbon dioxide. Recently COWLING [5] has also computed the emissivity at 286° K at pressure of one, a half, and a quarter atmosphere. COWLING's curve at one atmospheric pressure is therefore comparable with ours as was shown in fig. 10. It is to be seen that when u is smaller than nearly 0.1 cm his curve and ours nearly coincide, but when u increases beyond the value there arise considerable discrepancies between his curve and ours.

On his calculation, he writes : "The values are somewhat uncertain for large values of u for which absorption in the relatively transparent range 8-13 μ is important. Absorption in this range does not appear to vary with u in the way illustrated by table 1 (of his paper). Its run at atmospheric pressure can be estimated from ADEL's [7] diagrams."

Now I also used absorption coefficient of the range 9 - 13 μ determined from ADEL and LAMPLAND's measurements. Certainly as COWLING says, ADEL's experimented absorption curves for the range differ from COWLING's mean curve : they vary with u more steeply than COWLING's curve, but not so steep as the exponential law of absorption demands. So that I cannot understand why there happened to be such a large discrepancy between COWLING's curve and ours for large values of u. As far as I can understand, his curve should have been slightly higher than or nearly same as our curve.

In fig. 10 is also shown ROBINSON's curve which he claimes to be the curve for emissivity of water vapour alone obtained from observations. However it must be recalled that

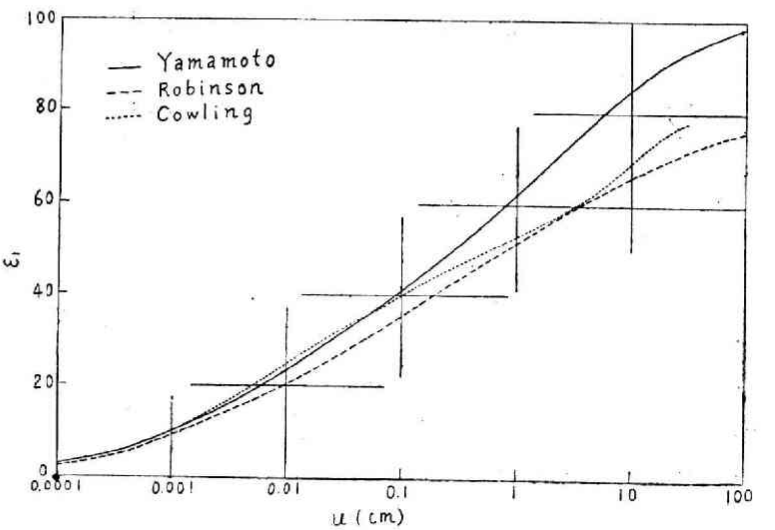

Fig. 10 Emissivity of column of water vapour without CO_2

he reduced 18.5 % as CO_2 absorption from his observed values. This procedure will necessarily mean considerable underestimation of absorption of water vapour when the quantity water vapour is large, because absorption coefficient of water vapour at infra-red CO_2 band is not so small. For example at 15 μ the value of l_ν is 0.44 ($T = 300°$ K), so that $l_\nu u/2 = 6.6$ for $u = 30$ and corresponding absorption of water vapour amounts to nearly 68 %. Thus it will not be reasonable to compare his curve with ours.

To check our calculation with ROBINSON's observation it is rather reasonable to take his emissivity curve of water vapour with CO_2 as the object of comparison. His orignal observations were carried out at several zenith angles which corresponds to different CO_2 contents. So that it is more reasonable to take his emissivity values of atmospheric slab which are shown in table 4 of his first report (1947) or in table 3 of his second report (1950) as the objects of comparison, because in atmospheric slab CO_2 content is constant, *i. e.*, equal to that contained in vertical air column. Further in comparison it must be noticed that in computing the reduced path he assumed ELSASSER's pressure correction, which will give rise to some overestimation of path. The degree of this overestimation can be known if we compute the reduced path of our meaning and that of ELSASSER's for several known distributions of humidity and pressure in the air column. This computations were carried out on model distributions given by LONDON [25] as average values for 0°−10°, 20°−30°, 30°−40°, 40°−50°, 50°−60° latitude belts in the northern hemisphere during March. (See appendix). As the result of computations we can roughly estimate that $u_p = 0.9\ u_{V\overline{P}}$, where u_p means the reduced path with our pressure correction and $u_{V\overline{P}}$, that with ELSASSER's pressure correction.

Now we computed the emissivity of a slab of water vapour with 116 cm of CO_2 which is assumed to exist in the vertical air column. The computation was carried out at 20°C using the values of l_ν at 300°K for the range of u larger than 0.3 cm which ROBINSON's measurments cover. The comparisons are shown in fig. 11, which shows that the computed curve is slightly higher than observed curves. However, the difference is so small that we may say that the computed emissivity is nearly in agreement with ROBINSON's observations. If we dare seek for the reason of the slight discrepancy, assuming ROBINSON's derivation of the emissivity of a slab from his observations on oblique air columns to be correct, (although there will be some questionable points on the derivation), in my opinion CO_2 absorption compiled by CALLENDAR seems to be slightly overestimated. In RUBENS and LADENBURG's experiment which was availed by CALLENDAR, the overestimation of absorption at the extremities of the band will probably exceed the underestimation of absorption at 14 - 16 μ for large path lengths, because absorption is nearly complete at the band ceutre for large path lengths.

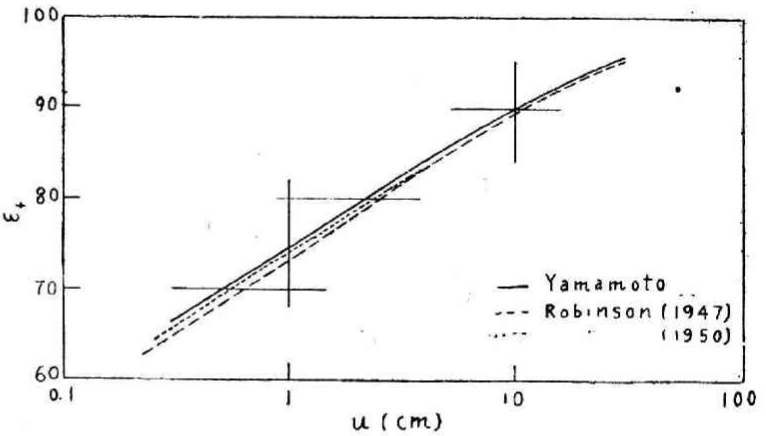

Fig. 11 Emissivity of slab of water vapour with CO_2

7. Downward Radiation at the Surface

Observations of doward radiation at the surface also give useful means of checking the validity of the chart. On this occasion we need to know the distributions with height, of temperature, pressure and humidity, during the observations to be able to know the reduced water path. Many classical observations of downward radiation are devoid of these data. Recent observations of ROBINSON are important ones which were carried out at known water paths, however it is regretted that in his papers sufficient description on air column conditions are lacking, so that we cannot at present carry out computations of downward radiation comparable with his observations. Hence the computations of downward radiation were carried out on the model distributions of LONDON already referred to. The distribution of CO_2 in the air column was assumed to be in accordance with table 2, and the computations were restricted on clear skies. The reduced water path, Δu, between any two successive levels, z_1 and z_2, is given by

$$\Delta u = \frac{\overline{p}}{p_0}\int_{z_1}^{z_2}\rho_w dz = \frac{\overline{q}}{g}\frac{\overline{p}}{p_0}\Delta p \qquad (28),$$

where $\overline{p}$, $\overline{q}$ are the average pressure and specifie humidity in the layer, ρ_w the density of water vapour, g the acceleration of gravity. By summing up the values of Δu from the reference level upward or downward, we can obtain the values of u. The results of computation of downward flux at the surface are shown in table 4, in which LONDON's computations using ELSASSR chart are also shown for comparison. It will be seen from the table that the computed values by ELSASSER chart are larger than those by our chart. Already ROBINSON has pointed out that the ELSASSER chart gives results too high by 6 to 14 per cent compared with his observations when the water path is small, but that it gives nearly correct values when the path length increeses. In table 4 are shown the percentage excess of computed by ELSASSER chart over that by our chart. The tendency for the excess to decrease with increasing path length is parallel to ROBINSON's description. From this fact we can expect, to some extent, the agreement of our computations with ROBINSON's observations.

In the table are also shown separately the contribution of water vapour alone and the additional contribution of carbon dioxide. With increase of water path the former increases and the latter decreases, as will be expected.

The downward radiation-water path relationship shown in the table is most favourably expressed by logarithmic law proposed by ELSASSER [2],

$$\frac{D}{\sigma T_0^4} = a + b\log_{10} u,$$

where $a = 0.732$, $b = 0.165$ for results by our chart and $a = 0.775$, $b = 0.117$ for those by ELSASSER chart.

Table 4 Average downward radiation at the surface for March, northern hemisphere, clear skies.

	u (cm)	T_0	$D/\sigma T_0^4$	$D_{H_2O}/\sigma T_0^4$	$D_{CO_2}/\sigma T_0^4$	$D^*/\sigma T_0^4$	$\frac{D^*-D}{D}$ (%)
0 - 10° N	3.87	300.9	0.820	0.779	0.041	0.839	2.3
20 - 30° N	2.33	295.5	0.788	0.733	0.055	0.818	3.8
30 - 40° N	1.40	286.2	0.757	0.687	0.070	0.790	4.25
40 - 50° N	0.95	277.2	0.726	0.647	0.079	0.774	6.6
50 - 60° N	0.51	268.2	0.683	0.589	0.094	0.744	8.9
60 - 70° N	0.25	258.9	0.631	0.521	0.110	0.701	11.1

D = downward radiation computed by YAMAMOTO

D_{H_2O} = contribution of water vapour

D_{CO_2} = additional contribution of CO_2

D^* = downward radiation computed by LONDON

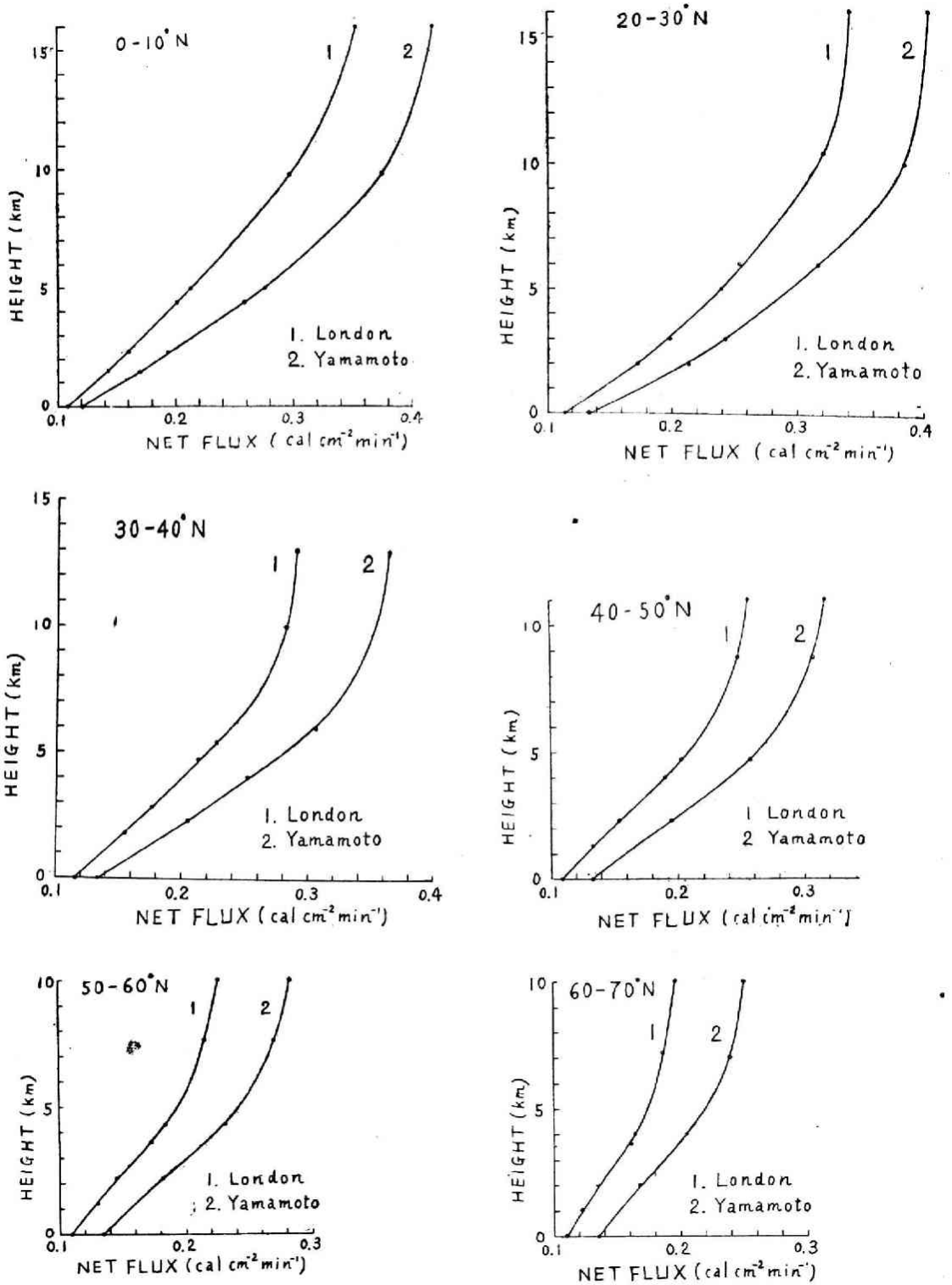

Fig. 12 Net infra-red flux in the troposphere for March, northern hemisphere, clear skies

8. Computations of Net Infra-red Flux in the Troposphere

Computations of net flux were also carried out on several cases of LONDON's model atmospheres assuming clear skies. The results are shown in fig. 12, in which LONDON's computations using ELSASSER chart are also shown for comparison. It will be seen that the values of net flux computed by our chart are larger than those computed by ELSASSER chart at every levels of every latitute belts. And the difference of values at given level increases with height. These differences will mainly be due to differently assumed CO_2 correction and pressure correction on each computation. It is disired that observations at higher levels will decide which of the two computations is nearer to truth.

Next, the rate of cooling of the troposphere by infra-red radiation was computed by the method described in LONDON's paper, *i. e.*,

$$\frac{dT}{dt} = 5.9 \times 10^3 \frac{\Delta F}{\Delta p}$$

where the rate of cooling dT/dt is in unit of degrees centigrade per day, ΔF is the infra-red flux difference in cal. cm^{-2}. min^{-1}. for a change in pressure Δp, in mb. The results are shown in fig. 13. Vertical distributions of cooling computed by LONDON and by the author are nearly similar.

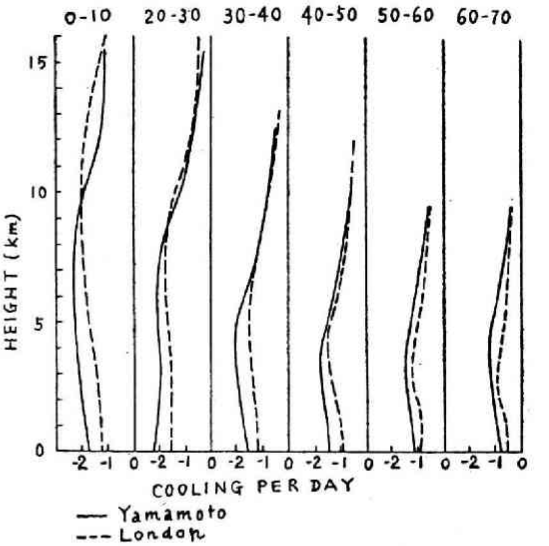

Fig. 13
Average infra-red cooling in the troposphere for March, northern hemisphere, clear skies.

9. Acknowledgement

The author expresses his thanks for the financial aid given by the Scientific Research Expenditure of Educational Department. He also thanks heartily to Miss T. NISHIMATSU and Miss S. SUZUKI for their helps on numerical computations.

References

(1) MÜGGE, R., and MÖLLER, F. : *Zeits. f. Geophys.* 8, 53, (1932)
(2) ELSASSER, W. M. : *Harvard Meteorological Studies*, No. 6, (1942)
(3) ROBINSON, G. D. : *Quart. J. Roy. Met. Soc.*, 73, 127 (1947) and 76, 37, (1950)
(4) DEACON, E. L. : *Australian J. Sci. Res., A.* 3, 274 (1950)
(5) COWLING, T. G. : *Phil. Mag.*, 3, 274, (1950)
(6) FOWLE, F. E. : *Astrophys. J.* 35, 149, (1912)
(7) ADEL, A. : *Astrophys. J.* 94, 451, (1941)
(8) YAMAMOTO, G. : *Sci. Rep. Tôhoku Univ.* Ser. 5, 3, 130, (1951)
(9) FOWLE, F. E. : *Smiths. Misc. Coll.* 63, No. 8, (1917)
(10) ADEL, A. and LAMPLAND, C. O. : *Astrophys. J.* 91, 481, (1940)
(11) WEBER, L. R. and RANDALL, H. M. : *Phys. Rev.* 40, 835, (1932)
(12) WEXLER, H. : *Mo. Wea. Rev.* 64, 122, (1936)
(13) YAMAMOTO, G and ONISHI, G. : *Sci. Rep. Tohoku Univ.* Ser. 5, 1, 5, (1949)
(14) GOODY, R. M. and ROBINSON, G. D. : *Quart. J. Roy. Met. Soc.*, 77, 151, (1951)
(15) KING, G. W., HAINER, R. M. and CROSS, P. C. : *J. Chem. Phys.*, 12, 210, (1944)
(16) VAN VLECK, J. H. and WEISSKOPF, V. F. : *Rev. Mod. Phys.*, 17, 227, (1945)
(17) BECKER, C. E. and AUTLER, S. H. : *Phys. Rev.*, 70, 300, (1946)

(18) CALLENDAR, G. S. : *Quart. J. Roy. Met. Soc.*, 67, 203, (1941)

(19) KAPLAN, L. D. : *J. Chem. Phys.* 15, 809, (1947) and 18, 186, (1950)

(20) MARTIN, P. E. and BARKER, E. F. : *Phys. Rev.*, 41, 291, (1932)

(21) RUBENS, H. and LADENBURG, E. : *Verh. d. D. Phys. Ges.*, 7, 170, (1905)

(22) FALCKENBERG, G. : *Met. Zeit.*, 56, 72, (1939)

(23) ELSASSER, W. M. : *Mo. Wea. Rev.*, 69, 1, (1941)

(24) BROOKS, F. A. : *Pap. Phys. Ocean. Met., Mass. Inst. Tech and Woods Hole Ocean. Inst.* 8, NO. 2, (1941)

(25) LONDON, J. : *U. S. Air Force Cambridge Res. Lab. Progress Rep.*, 131.01, 131.02 and 131.03, (1950)

Appendix

The distributions, compiled by LONDON, of pressure, temperature, relative humidity and shecific humidity in the northern hemisphere during March, were frequently used in our investigation, so that they were reproduced here with the distribution of reduced water path computed from them. In the table heights are given in km, pressure in mb, temperature in deg. cent., relative humidity in per cent, specific humidity in g/kg and reduced path in cm. In the last row of the table are shown aveage values in the lower stratosphere. The distributions for 10°-20°N were not used in our investigation, because they resemble to those for 0° - 10° N and 20°-30°N.

0 - 10° N						20 - 30° N					
Level	p	T	f	q	u	Level	p	T	f	q	u
0	1011	27.7	82	18.76	0	0	1017	22.3	72	11.86	0
1.0	902	22.8	68	13.03	1,683	1.0	904	16.5	64	8.25	1.10
1.5	858	20.6	63	11.09	2.153	2.0	792	10.3	54	5.32	1.75
1.8	830	19.2	60	10.00	2.422	2.6	742	7.2	48	4.09	1.932
2.0	808	18.2	59	9.50	2.615	3.0	707	4.7	43	3.23	2.0294
2.3	780	16.9	57	8.75	2.776	4.0	622	-1.0	37	2.08	2.1810
3.0	710	13.3	52	6.96	3.159	5.0	549	-6.7	34	1.34	2.2557
4.0	636	7.8	48	4.96	3.479	6.0	486	-12.3	32	0.874	2.2921
4.4	604	5.5	46	4.28	3.5772	7.0	427	-19.3	31	0.505	2.3108
5.0	562	2.0	44	3.43	3.6677	8.0	373	-26.5	30	0.277	2.3193
6.0	495	-3.5	41	2.36	3.7694	9.0	323	-33.8	30	0.148	2.3231
7.0	435	-10.0	39	1.46	3.8216	10.0	279	-41.3	31	0.0766	2.3245
8.0	385	-16.6	38	0.885	3.8475	10.4	262	-43.8	32	0.0630	2.3249
9.0	340	-23.2	37	0.518	3.8601	11.0	240	-47.7	34	0.0459	2.3252
9.8	302	-28.5	38	0.351	3.8648	12.0	204	-54.1	38	0.0266	2.3255
10.0	291	-30.0	38	0.312	3.8657	13.0	175	-60.7	45	0.0155	2.3256
11.0	253	-38.6	40	0.148	3.8681	14.0	149	-64.2	54	0.0135	2.3257
12.0	217	-47.2	43	0.0679	3.8690	15.0	125	-67.8	70	0.0125	2.3257
13.0	187	-55.7	49	0.0309	3.8694	16.0	107	-71.6	90	0.0109	2.3257
14.0	156	-62.3	58	0.0180	3.8695						
15.0	131	-69.0	70	0.0100	3.8696	above 16	62.5	-60.0	90		2.3258
16.0	112	-75.5	90	0.0054	3.8696						
above 16	65	-65	90		3.8697						

30 - 40° N						40 - 50° N					
Level	p	T	f	q	u	Level	p	T	f	q	u
0	1018	13.0	71	6.50	0	0	1017	4.0	75	3.73	0
1.0	903	9.0	60	4.75	0.627	1.0	899	1.0	70	3.18	0.394
1.8	830	5.4	54	3.63	0.894	1.3	875	0.0	68	2.95	0.460
2.0	810	4.4	52	3.34	0.9516	2.0	790	-3.0	65	2.44	0.6525
2.3	780	2.9	51	3.06	1.0284	2.3	760	-4.2	64	2.26	0.7075
2.8	727	0.2	49	2.60	1.1421	3.0	692	-7.7	61	1.76	0.8075
3.0	701	-1.0	48	2.40	1.1889	4.0	610	-14.0	58	1.08	0.8839
4.0	629	-6.3	45	1.61	1.2866	4.7	558	-19.0	57	0.730	0.9116
4.7	578	-10.4	43	1.17	1.3297	5.0	535	-21.0	56	0.616	0.9197
5.0	555	-12.4	43	1.02	1.3441	6.0	468	-28.0	54	0.338	0.9358
5.4	526	-15.0	42	0.832	1.3587	7.0	402	-35.0	52	0.181	0.9433
6.0	481	-19.2	42	0.613	1.3753	8.0	343	-41.8	52	0.0983	0.9464
7.0	415	-27.0	41	0.321	1.3892	8.7	308	-46.5	58	0.0702	0.9474
8.0	357	-34.8	42	0.168	1.3947	9.0	301	-47.5	60	0.0660	0.9475
9.0	307	-42.2	44	0.0893	1.3969	10.0	260	-53.7	72	0.0430	0.9482
10.0	270	-48.3	48	0.0532	1.3977	11.0	218	-55.0	90	0.0542	0.9486
11.0	226	-52.8	55	0.0424	1.3982						
12.0	193	-56.8	66	0.0340	1.3985	above 11	82.5	-50	90		0.9496
13.0	168	-60.0	90	0.0366	1.3986						
above 13	70	-55.0	90		1.3991						

50 - 60° N						60 - 70° N					
Level	p	T	f	q	u	Level	p	T	f	q	u
0	1015	-5.0	81	2.00	0	0	1015	-14.3	82	0.894	0
1.0	899	-7.5	75	1.70	0.207	1.0	895	-17.0	78	0.753	0.095
1.2	889	-8.0	74	1.61	0.2220	1.6	822	-18.7	75	0.670	0.1399
1.7	850	-9.7	71	1.40	0.2736	2.0	775	-20.0	73	0.610	0.1641
2.0	795	-10.8	70	1.34	0.3358	3.0	677	-23.3	69	0.480	0.2031
2.2	770	-11.6	69	1.26	0.3614	3.6	600	-26.7	66	0.368	0.2241
3.0	683	-15.3	65	0.962	0.4322	4.0	581	-29.0	65	0.296	0.2279
3.6	632	-19.0	62	0.701	0.4603	5.0	509	-34.0	62	0.190	0.2375
4.0	597	-21.5	61	0.575	0.4741	6.0	448	-38.2	60	0.131	0.2422
4.3	570	-23.5	60	0.485	0.4825	7.0	379	-42.0	62	0.104	0.2456
5.0	520	-27.9	59	0.336	0.4938	7.2	360	-42.7	63	0.102	0.2464
6.0	455	-33.7	57	0.202	0.5024	8.0	331	-45.5	68	0.0857	0.2473
7.0	390	-39.5	57	0.124	0.5069	9.0	285	-48.9	77	0.0739	0.2484
7.6	360	-42.5	59	0.0979	0.5084	10.0	245	-52.3	90	0.0662	0.2492
8.0	340	-44.5	62	0.0862	0.5090						
9.0	294	-49.5	73	0.0633	0.5101	above 10	83	-45	90		0.2505
10.0	252	-54.3	90	0.0511	0.5107						
above 10	84	-50.0	90		0.5118						